Generalization of Darcy's law for Bingham fluids in porous media: From flow-field statistics to the flow-rate regimes

Chevalier Thibaud* and Talon Laurent
Université Paris-Sud, CNRS, Laboratoire FAST, UMR 7608, Orsay F-91405, France
(Received 14 November 2014; published 13 February 2015)

In this paper, we numerically investigate the statistical properties of the nonflowing areas of Bingham fluid in two-dimensional porous media. First, we demonstrate that the size probability distribution of the unyielded clusters follows a power-law decay with a large size cutoff. This cutoff is shown to diverge following a power law as the imposed pressure drop tends to a critical value. In addition, we observe that the exponents are almost identical for two different types of porous media. Finally, those scaling properties allow us to account for the quadratic relationship between the pressure gradient and velocity.

DOI: 10.1103/PhysRevE.91.023011 PACS number(s): 47.56.+r, 47.50.−d, 47.53.+n, 89.75.Fb

Flows of non-Newtonian fluids through porous medium are of interest in many practical applications [1] such as ground reinforcement by cement injection, hydraulic fracturation, enhanced oil recovery (EOR) [2], or as a potential method for porosimetry [3]. Some of these fluids, such as mud, heavy oil, foam, emulsions, exhibit a yield stress [4]: they behave like liquid above a critical stress and as solid otherwise. Unlike Newtonian fluids, their flow characteristics in porous media are poorly known due to the interplay of the complex rheology and porous structure. Consequently, the determination of a macroscopic constitutive law to relate the flow rate to the applied pressure has been the subject of many investigations in the past [1,5–15] but remains a challenging and controversial issue [16,17].

For simple yield stress fluids (no thixotropy), the flow curve, i.e., the relation between steady state shear stress (τ) and shear rate ($\dot{\gamma}$), can be represented by the Herschel-Bulkley model

$$\tau < \tau_c \Rightarrow \dot{\gamma} = 0 \text{ (solid regime)},$$
$$\tau > \tau_c \Rightarrow \tau = \tau_c + k\dot{\gamma}^n \text{ (liquid regime)}$$

in which k and n are material parameters ($n = 1$ for a Bingham fluid) and τ_c is the yield stress. Based on experimental observations [5,6,13,18], the common law proposed in the literature between the flow rate and the applied pressure has the following form: $Q \propto (\Delta P - \Delta P_c)^n$, where Q is the mean flow rate, n is the Herschel-Bulkley power-law index, and ΔP_c a minimal pressure drop below which there is no flow. However, as demonstrated numerically in [19–21] for Bingham fluids, one should expect at least three different flowing regimes depending on the applied pressure (see Fig. 1). Those regimes can be interpreted by the progressive addition of flowing paths with the applied pressure. Indeed, just above the critical pressure, since only one flowing path is remaining, the flow rate evolves linearly with the pressure $Q \propto (\Delta P - \Delta P_c)$. This linearity results from the fact that inside this channel, the effective viscosity can be considered as constant (see [14]). For a larger applied pressure, more and more paths start to open progressively. It contributes then to enhance the flow rate according to a quadratic law $Q \propto (\Delta P - \Delta P_c)^2$. Finally, when the pressure is high enough, the fluid is yielded in the whole pore volume and behaves as a Newtonian one and the flow rate follows the standard Darcy's law (with a constant pressure loss coming from the fluid yield stress).

Since most of the experiments report only one flowing regime (with a pressure threshold) and were performed at significantly high net flow, we conjecture that it corresponds to the last regime. Moreover, this is supported by recent NMR experiments [16] which showed that the yield stress fluid flows in the whole pore volume for all the flow-rate values achieved experimentally.

The quadratic intermediate regime has instead been less investigated in particular to understand its range of observation, its exponent's origin, but also the impact of the porous medium disorder. Different arguments have been proposed in the literature to explain this quadratic dependence of the flow rate with the applied pressure. Roux and Herrmann [19] first observed this regime in a network of resistors with a threshold voltage and conjectured that the number of flow paths increased linearly with the pressure. Besides, Chen et al. [9] demonstrated that for a parallel tubes model with heterogeneous radii, the linearization of the probability distribution function (PDF) of the radii leads also to a quadratic flow rate. More recently, based on the work of [22] on percolation system, Sinha and Hansen [23] performed a mean field calculation on a capillary network leading to a quadratic dependence but also after linearizing the threshold PDF. If both models are based on the linearization of the PDF of the local pressure thresholds, it remains quite unclear why this argument holds for the whole range of pressure (i.e., from the first to the last channel to open).

The aim of this paper is to focus on this quadratic regime. In particular, we will demonstrate without any linearization of the distribution that this regime can be explained by the statistical properties of the unyielded regions.

I. NUMERICAL SIMULATIONS

Following the methodology of Talon and Bauer [21], we used a two relaxation time (TRT) lattice-Boltzmann scheme [24–26] to solve the two-dimensional (2D) Stokes flow of a Bingham fluid.

We employed the regularized effective viscosity proposed by Papanastasiou [27] (see also Mendes and Dutra [28]):

$$\nu_{\text{eff}}(\dot{\gamma}) = (1 - e^{-\dot{\gamma}/\dot{\gamma}_0})\tau_0\left(\frac{1}{2\dot{\gamma}} + \frac{1}{\dot{\gamma}_1}\right), \quad (1)$$

*Corresponding author: chevalier@fast.u-psud.fr

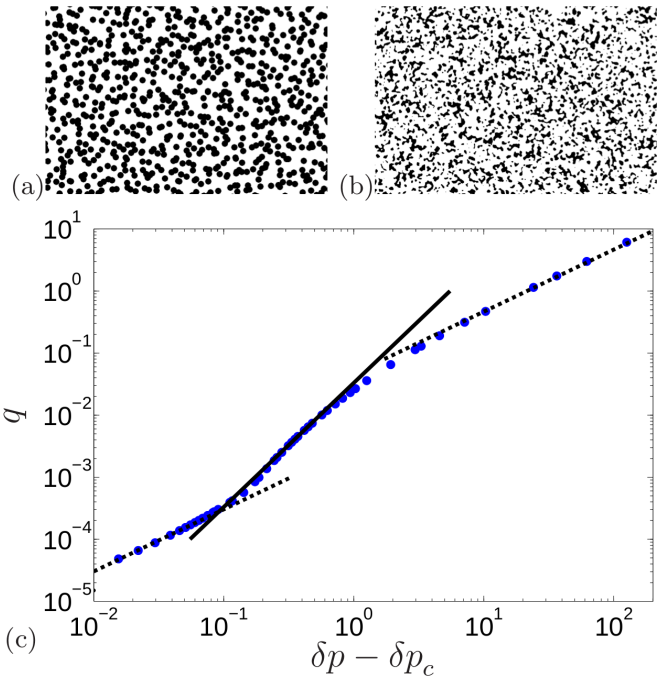

FIG. 1. (Color online) Top: disk packing (a) and stochastic (b) porous media. Bottom (c): dimensionless flow rate q as a function of the dimensionless distance to the critical pressure gradient $\delta p - \delta p_c$ in disk packing porous medium. The two dashed lines have a slope of 1 and the continuous line has a slope of 2.

where $\dot{\gamma}$ is the strain rate, τ_0 is the kinematic yield stress, $\dot{\gamma}_0$ is a regularizing parameter, and $\tau_0/\dot{\gamma}_1 = \nu_0$ defines the viscosity of the fluid.

We use two kinds of 2D porous media (see Fig. 1): a stochastic one, described in Talon and Bauer [21], and a random packing of monodispersed 2D disks, characterized by its correlation length (λ) and the disk radius (R), respectively.

In each realization, we imposed a pressure difference ΔP (with transverse periodic condition) and the mean flow rate Q is measured. The domain size was $L \times W = 4096 \times 1024$ where L and W are the length and width of the system; the numerical parameters can be found in [29]. All the variables used in this study have been made dimensionless by using the following characteristic quantities. The characteristic length l^* is the radius R for disk packing or λ for the stochastic media; the characteristic pressure is $p^* = \rho\tau_0$ and the characteristic velocity $v^* = l^* p^*/\rho\nu_0$. Thereby, we will denote δp and q the dimensionless pressure drop and flow rate, respectively. The dimensionless pressure threshold is denoted δp_c. We note also that the inverse of the dimensionless flow rate represents the Bingham number $Bi = q^{-1}$, i.e., the ratio of the yield stress (τ_c) to the viscous stress ($k\dot{\gamma}^n$).

II. RESULTS

The flow paths, extracted from the 2D velocity map, are represented (in white) on Fig. 2 for different applied pressure drops. They border regions of unyielded nonflowing fluid which are identified by different color shades. In this figure, one can distinguish two important features: the clusters' area decreases as the flow rate increases and its distribution seems

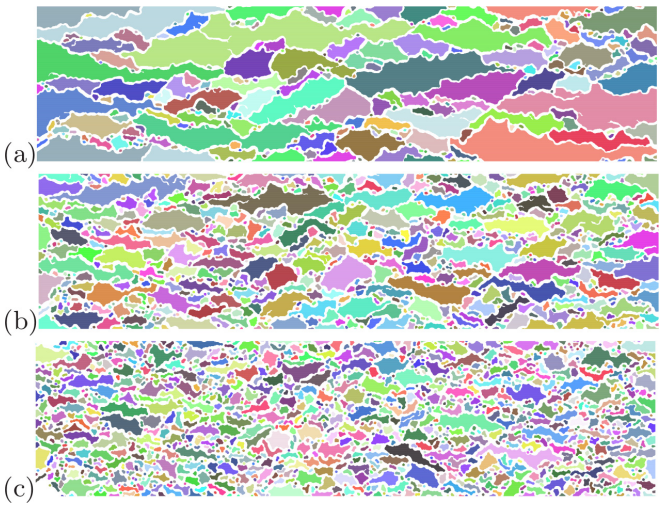

FIG. 2. (Color online) Clusters of nonflowing regions (colored patches) for different dimensionless flow rates (from top to bottom: $q_a = 2.5 \times 10^{-3}, q_b = 10^{-2}, q_c = 2.7 \times 10^{-2}$) in the disk packing geometry. The active flow paths appear in white.

to be large. We note that those features are reminiscent of critical phenomena, particularly the percolation.

For each cluster, the following characteristics have been extracted: the area S and, from the smallest rectangle containing it, their length l and width w. We plot the probability distributions of cluster size on Fig. 3 for different imposed pressure drop in disk packing (we have excluded clusters touching the inlet and the outlet). For statistical reasons, it was performed with an average over five realizations for disk packing porous medium.

It can be seen that $p(S)$ follows reasonably a power-law decay (with exponent $\tau = 1.46 \pm 0.06$ and 1.5 ± 0.05 for disk packing and stochastic porous media, respectively), with a cutoff at large sizes. We note that the stochastic porous medium displays another power-law decay at low sizes ($S \lesssim 1$) with an exponent $-\frac{1}{2}$. We attribute this behavior to the distribution of solid sizes. Indeed, in our determination procedure, the solid sites are included in our nonflowing clusters which is more distributed for the stochastic media than the disk packing. Moreover, for each flow rate, the distribution could be well fitted by

$$p(S) \propto S^{-\tau} \exp\left(-S/S_0\right). \tag{2}$$

The inset of Fig. 3 provides the evolution of this cutoff size, estimated by measuring the maximum size S_0 in the system, which reduces while the flow rate increases. At low and high flow rates, S_0 reaches its limits, determined, respectively, by the system and the pore sizes. In-between, we found a power-law decay with q (and also with the pressure difference, not shown):

$$S_0 \propto (\delta p - \delta p_c)^{-\chi} \propto q^{-\gamma} \tag{3}$$

with $\gamma = 1$ (see Table I for fitting error). It is worth mentioning that it was more convenient to present scaling laws with respect to the flow rate q rather than the pressure difference $\delta p - \delta p_c$. The latter induces more errors due the requirement of δp_c

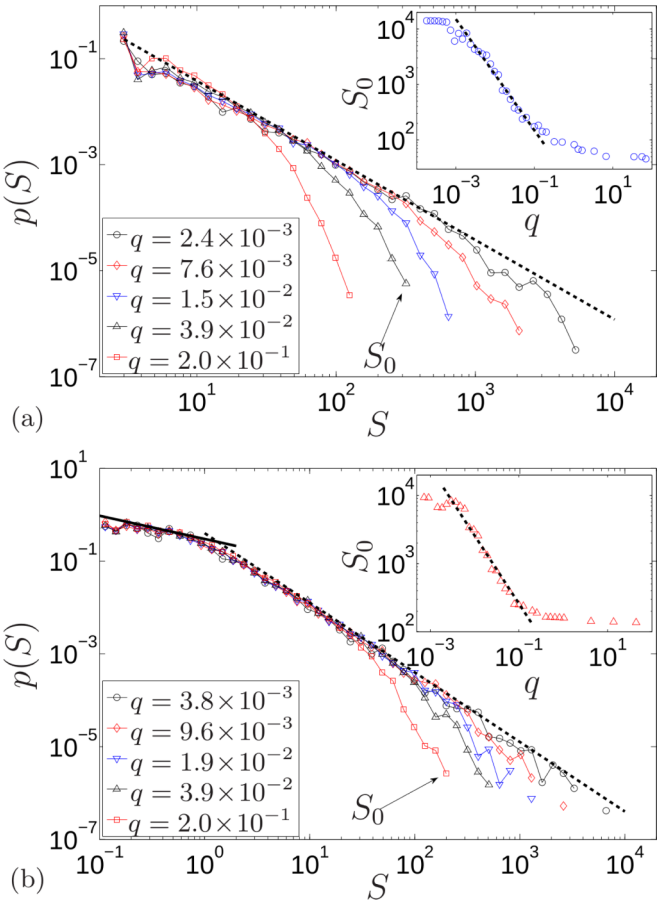

FIG. 3. (Color online) Nonflowing cluster size PDF $p(S)$ in disk packing (a) and stochastic (b) porous media for different flow rates. The dashed line is a fit of the form: $p(S) \propto S^{-\tau}$ with $\tau = \frac{3}{2}$. Solid line (b): variations as $S^{-1/2}$. Inset: flow-rate dependence of the cutoff cluster area S_0 (S_0 is the maximal cluster area at each given flow rate). The dashed line is a guide for the eye, $S_0 \propto q^{-\gamma}$ with $\gamma = 1$.

which depends on the realization and is subject to numerical errors (see the regularization errors described in [21]). Thus, in order to present statistical properties, it is more convenient to average realizations with the same flow rate than the same distance to the critical pressure.

Combining (2) and (3) allows us to deduce a scaling function for the PDF:

$$p(S) \propto q^{\gamma\tau} f(Sq^{\gamma}) \qquad (4)$$
$$\text{with} \quad f(x) = x^{-\tau} e^{-x}.$$

TABLE I. Fitted value of the exponents and error.

Law	Exponent	Bead	Stochastic
$p(S) \propto S^{-\tau}$	τ	1.46 ± 0.06	1.5 ± 0.05
$S_0 \propto q^{-\gamma}$	γ	0.97 ± 0.07	1.1 ± 0.1
$p(l) \propto l^{-\beta}$	β	1.75 ± 0.1	1.85 ± 0.05
$l_0 \propto q^{-\xi}$	ξ	0.60 ± 0.05	0.70 ± 0.1
$w \propto l^{\alpha}$	α	0.66 ± 0.03	0.69 ± 0.03
$S \propto l^{\phi}$	ϕ	1.59 ± 0.09	1.64 ± 0.06

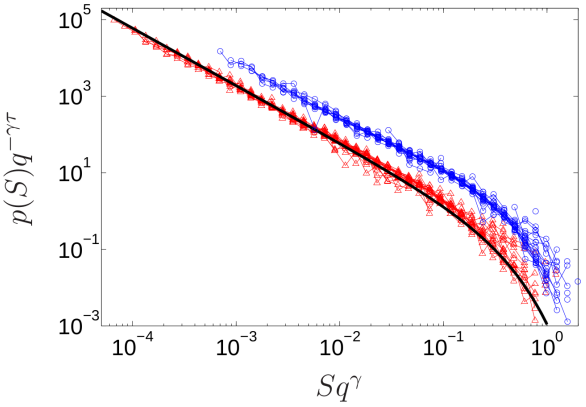

FIG. 4. (Color online) Normalized probability distributions of nonflowing cluster size PDF $p(S)$ in disk packing (blue upper circle) and in stochastic (red bottom triangle) porous media with $\gamma = 1$ and $\tau = \frac{3}{2}$. The continuous curve represents $y \propto x^{-3/2}\exp(-x)$.

Figure 4 displays, for the two kinds of porous media, this scaling function for $\tau = \frac{3}{2}$ and $\gamma = 1$ at different flow rates belonging to the quadratic regime (i.e., the maximum cluster size has not reached one of the two bounds). To obtain the normalized probability distributions of nonflowing cluster in the stochastic porous medium, we remove the low sizes part ($S \lesssim 1$) as it does not follow the same power-law decay as the one used in the scaling function. Remarkably, one can note that the data collapse works remarkably well. Another remarkable point is the independence of this scaling function and exponents with the type of disorder. This suggests that the present problem displays universal statistical characteristics.

Interestingly, other statistical properties of the clusters exhibit similar behaviors. For instance, the probability distribution of the lengths l follows the same kind of scaling law: $p(l) \propto l^{-\beta} \exp(-l/l_0)$ where l_0 is the cutoff length: $l_0 \propto q^{-\xi}$ (see Fig. 5).

Another important geometrical property of the clusters is the aspect ratio. We first calculate the mean width and area for a given length: $\langle w \rangle_l$ and $\langle S \rangle_l$. For the two kinds of porous media, we observe on Fig. 6 that at all flow rates, the cluster aspect ratio displays a self-affine property, namely, $\langle w \rangle_l \propto l^{\alpha}$, with $\alpha \simeq \frac{2}{3}$. This self-affinity shows then that at very large scale, the aspect ratio (w/l) of the clusters tends to be zero (flat). We also note that the scaling deviates from this power law at scales of the order of the solids length scale, particularly for the stochastic medium.

Table I summarizes the different observed power laws along with the corresponding exponents. The most remarkable result is that all those exponents are very similar for the two different types of disorder. This might then support the contention of a universal behavior. It is also worth noting that all those exponents are not independent between each other. Indeed, one can find three dependence relationships. First, assuming that the surface of a cluster is proportional to lw leads to

$$S \propto l^{\phi} \qquad (5)$$

with $\phi = \alpha + 1$. This assumption is validated on Fig. 7. Second, this last relationship (5) and the two power-law distribution functions $p(S) \propto S^{-\tau}$ and $p(l) \propto l^{-\beta}$ yield to

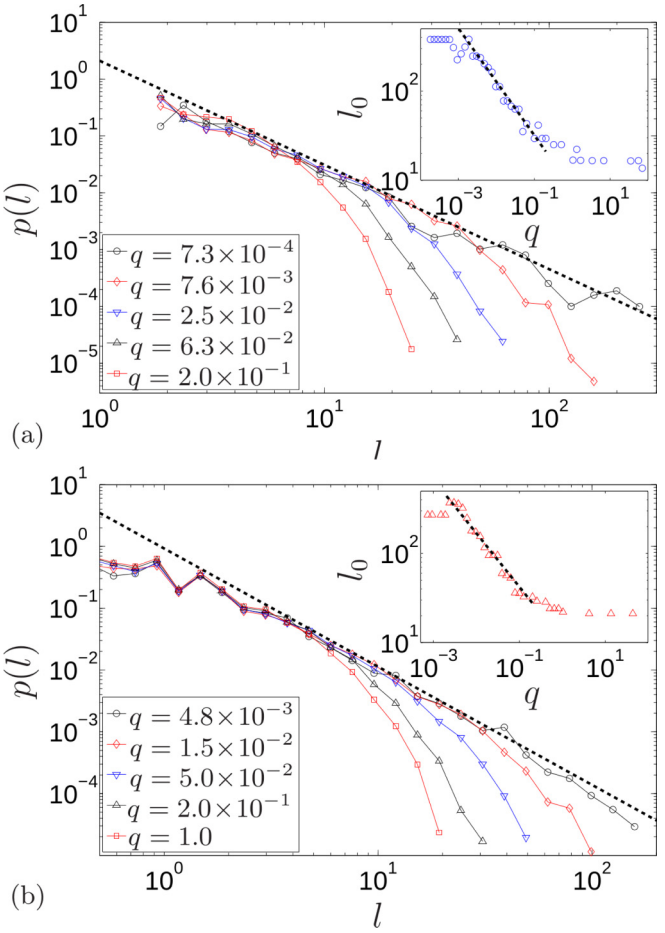

FIG. 5. (Color online) Nonflowing cluster length PDF $p(l)$ in disk packing (a) and stochastic (b) porous media for different flow rates. The dashed line is a fit of the form $p(l) \propto l^{-\beta}$ with $\beta = \frac{11}{6}$. Inset: flow-rate dependence of the cutoff cluster length l_0 (l_0 is the maximal cluster length at each given flow rate). The dashed line is a guide for the eye, $l_0 \propto q^{-\xi}$ with $\xi = \frac{3}{5}$.

$\beta = \tau(\alpha + 1) - \alpha$. Finally, (5) leads to the cutoff size exponent relation $\xi = \gamma/(\alpha + 1)$. From those three relationships, we can infer that only three exponents are independent (we choose τ, γ, α) and that all the other exponents can be derived

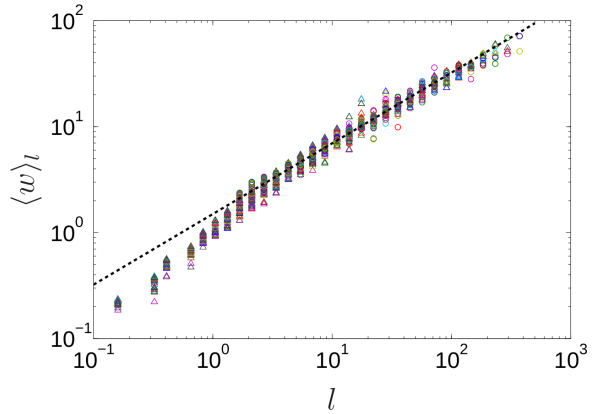

FIG. 6. (Color online) Average clusters width as a function of their length in disk packing (circle) and in stochastic (triangle) porous media for different flow rates. The dashed line scales as $\langle w \rangle_l \propto l^{2/3}$.

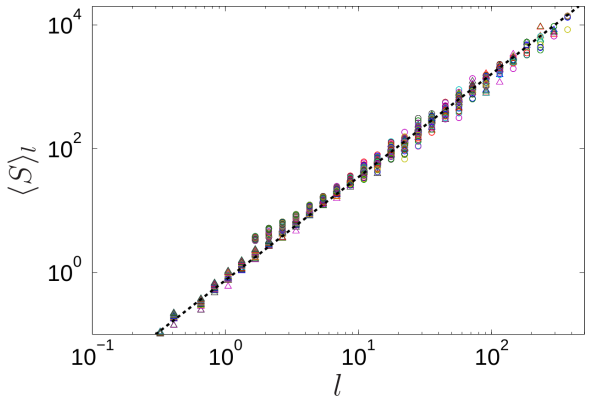

FIG. 7. (Color online) Average clusters area as a function of their length in disk packing (circle) and in stochastic (triangle). The dashed line scales as $\langle S \rangle_l \propto l^{5/3}$.

from them. In Table II, we derived the exponents from the previous relationships, which are more than consistent with the measurements.

III. SCALING FLOWING REGIME

In this section, we aim to relate the previously statistical properties of the clusters to the quadratic flowing scaling regime. Indeed, following Roux and Herrmann [19], one can reasonably assume that the total flow rate is proportional to the total number of flowing channels (N_{chan}), which is in fact the assumption made to derive the Kozeny-Carman's law [30]. N_{chan} can then be approximated to the number of clusters (N), which can be derived from average cluster size and the total system area: $N = A/\langle S \rangle$. From the distribution (2), the average cluster size can be computed:

$$\langle S \rangle = \int_0^\infty S p(S) dS = {S_0}^{-\tau+2} \Gamma(2-\tau) \propto q^{\gamma(\tau-2)} \Gamma(2-\tau), \tag{6}$$

where Γ is the gamma function. Applying Darcy's law leads then to

$$q \propto K(q)(\delta p - \delta p_c) \propto A q^{-\gamma(\tau-2)} (\delta p - \delta p_c).$$

Finally, we obtain the flow-rate–pressure relationship $q \propto (\delta p - \delta p_c)^\mu$ with $\mu = 1/[1 + \gamma(\tau - 2)] = 2.1 \pm 0.2$, which gives the correct scaling law within the error bar. We note, however, that the error bar is rather large, mainly due to the determination of γ. Its reduction would have required us to increase significantly the system size.

TABLE II. Exponents derived from the set (τ, γ, α).

Law	Exponent	Bead	Stochastic
$p(l) \propto l^{-\beta}$	$\beta = (\alpha+1)\tau - \alpha$	1.76 ± 0.15	1.85 ± 0.14
$l_0 \propto q^{-\xi}$	$\xi = \gamma/(\alpha+1)$	0.58 ± 0.07	0.65 ± 0.09
$S \propto l^{\phi}$	$\phi = \alpha + 1$	1.66 ± 0.03	1.69 ± 0.03
$q \propto (\delta p - \delta p_c)^{\mu}$	$\mu = 1/(1 + \gamma(\tau - 2))$	2.1 ± 0.2	2.2 ± 0.3

IV. DISCUSSION AND CONCLUSION

In this paper, we have investigated the quadratic regime of the flow-rate–pressure relationship, where the apparition of the flow paths increases with the applied pressure drop. From a statistical point of view, we have shown that the distribution of the unyielded clusters exhibits similar behavior as for a second order critical phenomenon. The imposed pressure and the net flow rate would then be, respectively, the control and order parameter.

The most salient feature is that the cluster's size is distributed according to a power law with a cutoff at large size which depends on the flow rate (or the distance to the critical pressure). The lower and upper bounds of this cutoff are, respectively, the local characteristic scale of the porous medium and the size of the system. It is worth noting that those two bounds are reached roughly at the beginning and at the end of the second flowing regime observed on Fig. 1. This can be physically understood since when only few flow paths remain, the largest clusters reach the two boundaries. On the other hand, when the maximum cluster reaches the pore size, it corresponds to the situation where very few areas remain unyielded. The saturation of the maximum cluster size can then give another interpretation of the range of the quadratic flow-rate regime.

We have investigated two different kinds of porous media which are observed to share the same scaling exponents. This could suggest the "universality" of those exponents. It is, however, important to note that the present exponents differ significantly from the percolation theory. In particular, it would have led to the exponents (see [31]) $\tau \simeq 2.03$ and $\alpha = 1$ (fractal).

Finally, we have shown that those exponents allow us to predict remarkably well the correct scaling of the flow-rate–pressure relationship. It also confirms and explains the physical conjecture proposed by [19], who assumed that the number of channels increases linearly with the increase of pressure. Indeed, two effects are at work. First, the number of channels is determined by the cutoff size [from Eq. (6)] with an exponent $S_0^{-2+\tau}$. And second, this cutoff size diverges with the distance to the threshold with another exponent $S_0 \propto q^{-\gamma}$. It is then very surprising and fortuitous that the nonlinear combination of those two exponents leads to the validation of this simple conjecture.

Further works will be dedicated to investigate other types of disorder (pore distribution, anisotropy, 3D, etc.). It seems indeed very important to characterize the "universality" of the presented exponents and the resulting flowing-pressure relationship. The extension of this work to three-dimensional porous media seems to be a challenging but very interesting problem. For instance, we expect that the branching structure will not define closed volumes of immobile regions. This topological property should then require us to revisit the methodology presented in this paper.

ACKNOWLEDGMENTS

The authors would like to thank A. Hansen, J.-P. Hulin, and D. Salin for useful discussions and the Agence Nationale de la Recherche for financial support of the project LaboCothep No. ANR-12-MONU-0011.

[1] J. Savins, Ind. Eng. Chem. **61**, 18 (1969).
[2] J. Pearson and P. Tardy, J. Non-Newtonian Fluid Mech. **102**, 447 (2002).
[3] A. Ambari, M. Benhamou, S. Roux, and E. Guyon, C. R. Acad. Sci., Ser. II **311**, 11 (1990) (in French).
[4] P. Coussot, *Rheometry of Pastes, Suspensions, and Granular Materials: Applications in Industry and Environment* (Wiley, Hoboken, NJ, 2005).
[5] H. C. Park, M. C. Hawley, and R. F. Blanks, Polymer Engineering & Science **15**, 11 (1975).
[6] T. Al-Fariss and K. L. Pinder, Can. J. Chem. Eng. **65**, 391 (1987).
[7] G. G. Chase and P. Dachavijit, Sep. Sci. Technol. **38**, 745 (2003).
[8] M. T. Balhoff and K. E. Thompson, AIChE J. **50**, 3034 (2004).
[9] M. Chen, W. Rossen, and Y. C. Yortsos, Chem. Eng. Sci. **60**, 4183 (2005).
[10] T. Sochi and M. J. Blunt, J. Pet. Sci. Eng. **60**, 105 (2008).
[11] X. Clain, Étude expérimentale de l'injection de fluides d'Herschel-Bulkley en milieux poreux, Ph.D. thesis, Université Paris-Est, 2010.
[12] M. Balhoff, D. Sanchez-Rivera, A. Kwok, Y. Mehmani, and M. Prodanović, Trans. Porous Media **93**, 363 (2012).
[13] T. Chevalier, C. Chevalier, X. Clain, J. Dupla, J. Canou, S. Rodts, and P. Coussot, J. Non-Newtonian Fluid Mech. **195**, 57 (2013).
[14] L. Talon, H. Auradou, and A. Hansen, Front. Phys. **2**, 24 (2014).
[15] A. de Castro, A. Omari, A. Ahmadi-Snichault, and D. Bruneau, Trans. Porous Media **101**, 349 (2014).
[16] T. Chevalier, S. Rodts, X. Chateau, C. Chevalier, and P. Coussot, Phys. Rev. E **89**, 023002 (2014).
[17] J. Bleyer and P. Coussot, Phys. Rev. E **89**, 063018 (2014).
[18] G. Chase and P. Dachavijit, Rheol. Acta **44**, 495 (2005).
[19] S. Roux and H. J. Herrmann, Europhys. Lett. **4**, 1227 (1987).
[20] L. Talon, H. Auradou, M. Pessel, and A. Hansen, Europhys. Lett. **103**, 30003 (2013).
[21] L. Talon and D. Bauer, Eur. Phys. J. E **36**, 1 (2013).
[22] S. Kirkpatrick, Rev. Mod. Phys. **45**, 574 (1973).
[23] S. Sinha and A. Hansen, Europhys. Lett. **99**, 44004 (2012).
[24] I. Ginzburg and K. Steiner, Philos. Trans. R. Soc., A **360**, 453 (2002).
[25] I. Ginzburg, F. Verhaeghe, and D. A. d'Humières, Commun. Comput. Phys. **3**, 427 (2008).
[26] I. Ginzburg, F. Verhaeghe, and D. A. d'Humières, Commun. Comput. Phys. **3**, 519 (2008).
[27] T. C. Papanastasiou, J. Rheol. **31**, 385 (1987).
[28] P. S. Mendes and E. S. Dutra, Appl. Rheol. **14**, 296 (2004).
[29] We used, in numerical units, for the disk packing $R = 8.5$, $\tau_0 = 6.67 \times 10^{-8}$, $\dot{\gamma}_1 = 1.33 \times 10^{-5}$, $\dot{\gamma}_0 = 10^{-5}\dot{\gamma}_1$ and for the stochastic medium $\lambda = 6$, $\tau_0 = 3.85 \times 10^{-8}$, $\dot{\gamma}_1 = 7.69 \times 10^{-6}$, $\dot{\gamma}_0 = 10^{-5}\dot{\gamma}_1$.
[30] J. Bear, *Dynamics of Fluids in Porous Media* (Elsevier, New York, 1988).
[31] D. Stauffer and A. Aharony, *Introduction to Percolation Theory* (Taylor and Francis, London, 1991).